JOURNAL OF MATERIALS SCIENCE 26 (1991) 5195–5202

Solid state transformations in Fe–Ni supercooled alloys

A. MUNITZ
Nuclear Research Centre-Negev, P.O. Box 9001 Beer-Sheva, Israel
M. TALYANKER
Ben-Gorion University, Beer-Sheva, Israel
G. J. ABBASCHIAN
University of Florida, Gainesville, Florida 32611 USA

The effect of supercooled microstructures and composition in the solid state transformation of the Fe–Ni system was investigated utilizing transmission electron microscopy (TEM), and scanning electron microscopy (SEM). Irrespective of the supercooling degree, Fe–Ni samples containing between 7 and 28 wt % Ni underwent a martensitic transformation above room temperature. The martensite morphology is superimposed on the sub-grain microstructure obtained by supercooling. Indications exist that alternative nucleation is activated if the samples are supercooled below the δ–T_0 curve. The impact of alternative nucleation on the martensitic transformation is discussed. Coherent precipitation was observed in Fe–33 wt % Ni alloys. The precipitate dimensions depend on the solidification path. The results are discussed in terms of current supercooling theories.

1. Introduction

The hardening of steel due to a martensitic transformation resulting from rapid cooling from a high temperature is probably the most effective simple heat treatment ever devised. The martensitic transformation combined with a suitable thermo-mechanical treatment has great engineering importance. Similar processes have led to the development of the strongest non-brittle material available, i.e. the maraging steel, which has a maximum ultimate tensile stress of 3500 MPa (about 0.3 of the theoretical limit for defect-free iron). The Fe–Ni system has been the subject of intensive investigations due to the relative ease with which martensitic transformations in these alloys can be observed. The investigations were aimed at understanding the nucleation kinetics of the martensitic formation, its morphology and crystallography [1–3].

Fe–Ni martensite has a plate-like morphology [3] which is always at least partially twinned, with the amount of twinning increasing with nickel concentration or decreasing with the martensite start temperature (M_s). It was also found [1], that the M_s temperature is a decreasing function of the Ni content in the Fe–Ni alloy. The M_s temperature decreases below room temperature in Fe–Ni containing more than 28 wt % Ni. However, there is only meagre information on the effects of supercooled microstructures and composition on the solid state transformation. The major part of the works are dedicated to investigating the effects of supercooling on the solute distribution and microstructure in Fe–Ni alloys [4–8]. It has been found that the sub-grain microstructure in Fe–Ni alloys fall into four major categories [9]: dendritic, spherical, mixed dendritic and spherical, and "rosettes". The appearance of a specific structure depends solely on the degree of supercooling [9, 10]. The microsegregation profiles of supercooled samples were also found to be substantially different from those of conventionally solidified materials.

The aim of the present work was to obtain better understanding of solid state transformations in the Fe–Ni system of microsegregational profiles and microstructures produced upon supercooling conditions. The effect of supercooling on the nucleation of alternate γ–Fe or δ–Fe phases was of particular interest.

2. Experimental procedure

Fe–Ni samples were melted in an electromagnetic levitation apparatus, supercooled and quenched, as described in detail elsewhere [9, 10]. The nominal composition of the alloys studied and the maximum supercooling obtained for each alloy are summarized in Table I. Processed samples were cut into rectangles and used for metallography, and electron microscopy. The specimens for transmission electron microscopy were first abraded to 100 μm thickness, from which discs of 3 mm diameter were punched out. The discs were electropolished with 10% perchloric acid in acetic acid using a voltage of 30–40 V. After electropolishing, the samples surfaces were cleaned using an ion miller at 5 KV for 2 min.

0022–2461/91 $03.00 + .12

TABLE I Summary of the sample composition and the maximum supercooling obtained.

Composition (wt %) Ni	Maximum supercooling obtained (K)
7	220
10	220
15	230
24	320
33	190
45	200

The microstructure and microsegregation profiles of the samples were studied using scanning electron microscopy (SEM). For SEM examination, the samples were mechanically polished using diamond pastes of up to 6 μm fineness. They were then electropolished using a solution of 10% perchloric acid in acetic acid at room temperature and a voltage of 40 V for 10–15 seconds. After the electropolishing the specimens were lightly etched in order to reveal the microstructure while keeping geometrical effects during compositional analysis to a minimum. Ni and Fe compositional line profiles were taken using an energy dispersive spectroscopy (EDS) system at 25 kV, across the dendrite element width at 5–15 locations throughout the sample. Each line profile consisted of 20 points, 1 μm apart. The raw data were corrected with a standard "ZAF" computer program (Z-atomic number, A-absorption, and F-fluorescence, plus background and dead time corrections).

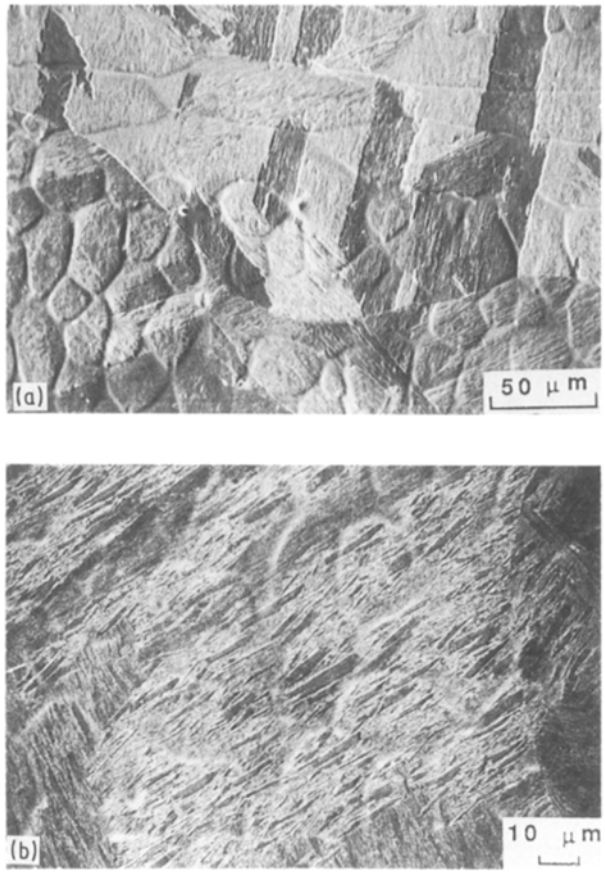

Figure 1 Secondary electron images illustrating the sub-grain microstructure of Fe 15 wt % Ni at different supercooling. The martensite morphology is superimposed on the sub-grain morphology. (a) 100 K supercooling; and (b) 160 K supercooling.

3. Results

The revealed microstructure of supercooled Fe–Ni alloys at room temperature is a result of the combined effects of the martensitic transformation and supercooling. It has been found that the sub-grain microstructure in Fe–Ni alloys fall into four major categories [9] according to the degree of supercooling: dendritic, spherical, mixed dendritic and spherical, and "rosettes". When supercooling was less than 170 K prior to nucleation, the resulting microstructure of the solid was predominantly dendritic. However, spherical and mixed dendritic and spherical regions were also observed. At supercooling ranging between 170 and 220 K, the microstructure consisted of a spherical morphology, whereas at supercooling larger than 220 K, the morphology gradually changed toward a "rosette' type structure [9, 10]. After solidification, upon cooling to room temperature, Fe–Ni alloys containing between 7 and 28 wt % Ni underwent a martensitic transformation irrespective of the supercooling degree. This is seen in Figs 1 and 2. In Fig. 1 we show secondary electron images of Fe 15 wt % Ni for supercooling degrees of 100 K, and 160 K, respectively. Both exhibit a dendrite element morphology. The martensitic morphology is superimposed on the sub-grain structure as illustrated in Fig. 1. The martensitic morphology of alloys supercooled below the δ–T_0 curve (the curve on which the free energy of the solid equals the free energy of the liquid), as reported by Kelly and Vander Sande [11] is different from the morphology of an alloy which was supercooled above the δ–T_0 curve, as illustrated for Fe 15 wt % Ni (Fig. 1). For this composition, the δ–T_0 temperature is about 155 K below the liquidus temperature. The microstructure shown in Fig. 1a represents the martensite morphology of alloys which nucleated above δ–T_0, while Fig. 1b exhibits microstructure of alloys supercooled below δ–T_0. The latter martensite is finer, with some rectangular shapes embedded. In Fig. 2, we show secondary electron images demonstrating the martensite microstructure of the Fe–25 wt % Ni which was dropped from the solid + liquid zone. As expected under such solidification conditions, the solidification proceeds in a dendritic manner. Since the sample solidified with no supercooling, the minimum in Ni concentration occurs, according to Scheil's equation, in the centre of the dendritic cell, while at the circumference it increases above the C_0 composition of Ni. X-ray microanalysis shows that the centre of these dendrites contains about 23 wt % Ni and has a martensitic morphology, while the outer smooth part contains about 27.5 wt% Ni, and a martensite morphology could not be observed (see Fig. 2). This indicates that the local and not the overall composition is the main factor determining whether martensitic transformation will take place.

Supercooling also affects the solute distribution inside the dendrite element. In Fe–Ni alloys, which

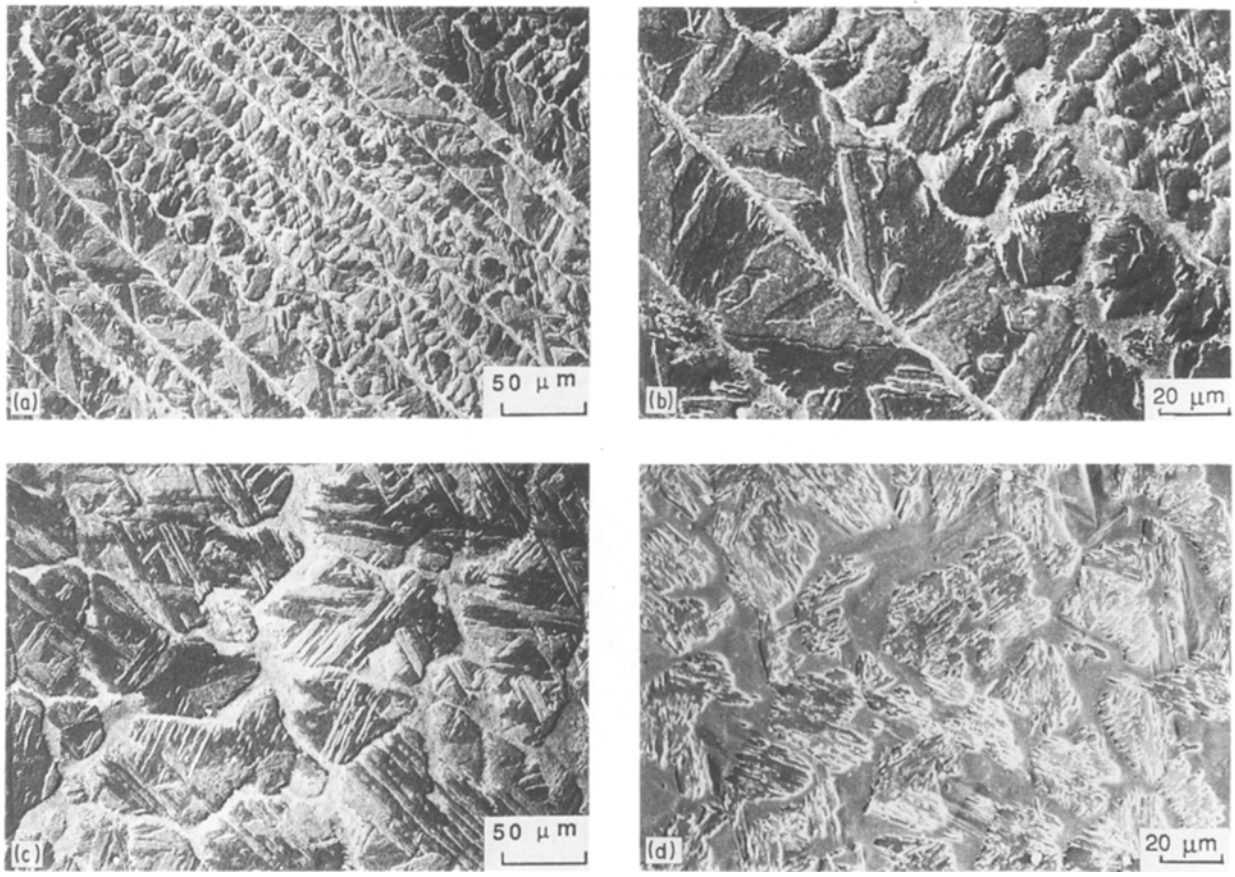

Figure 2 Secondary electron images showing the microstructure of Fe–25 wt % Ni which was dropped from the solid + liquid zone at different magnifications.

were supercooled below γ–T_o but above the δ–T_o curve, one can observe crosses in the middle of each dendrite element as in Fig. 3. In Fig. 3a to c, we show secondary electron images illustrating the microstructure of Fe–Ni samples supercooled by 60 K containing 15, 33.3 and 45 wt% Ni, respectively. Microprobe X-ray analysis has shown that the crosses in the interior of the dendrite elements, marked by arrows, are Ni-rich areas formed as a result of a partitionless solidification [9, 10] and the surroundings are solute-poor regions which solidified after partitioning occurred. In samples which contain 15 wt % Ni, the martensite morphology is superimposed on the solute Ni-rich crosses (Fig. 3a). The observation of the crosses is difficult when the martensite exists in the sample. However, upon careful etching one can expose both phenomena. In supercooled samples which contained 33.3 and 45 wt % Ni, martensite morphology could not be observed, as illustrated in Fig. 3b and c. Note that above 28 wt % Ni, the martensite start temperature, M_s is below room temperature. X-ray diffraction indicates that only the γ–Fe phase exists at room temperature, while in Fe–15 wt % Ni one could observe both fcc and bcc phases. The crosses also could not be observed in samples which were supercooled below δ–T_o (Fig. 1b). It was found that in such cases the solute (Ni) concentration is markedly different from the solute concentration in the case when the sample nucleated above the δ–T_o curve. A comparison between the Ni concentration line profile across a dendrite element which was supercooled above δ–T_o (containing crosses in the dendrite element) and below δ–T_o (with no crosses observed) is shown in Fig. 4 for Fe–8.7 and 14.7 wt % Ni alloys. As illustrated in Fig. 4a, in the sample which was supercooled below γ–T_o but above δ–T_o, the dendrite elements contained central solute-rich crosses of the initial alloy composition. On the other hand, alloys which were supercooled below δ–T_o did not show these solute-rich crosses. The Ni composition line profiles exhibit a plateau at the central part of the dendrite element across most of the element cross-section, then the concentration increases monotonically towards the periphery (Fig. 4b). The Ni concentration in the central part of the element fluctuates. It should be noted that, although the compositional Ni line profiles in this case are similar to those of alloys solidified with no supercooling, the minimum concentration level on the former is much higher. The transmission electron micrographs in Fig. 5 demonstrate the effect of supercooling by 210 K prior to quenching on the microstructure of Fe–8 wt % Ni alloys. The microstructure consists of a lath martensite. Analysis of selected area diffraction patterns taken from successive plates indicated that the microstructure consists of α' martensite, plates which alternate with approximately parallel γ plates. X-ray microanalysis on the successive plates shows that both structures contain the same Ni concentration. Similar microstructures were observed in samples solidified under different supercooling levels. In Fe–8 wt % Ni specimens solidified with supercooling exceeding 90 K (supercooled below the δ–T_o)

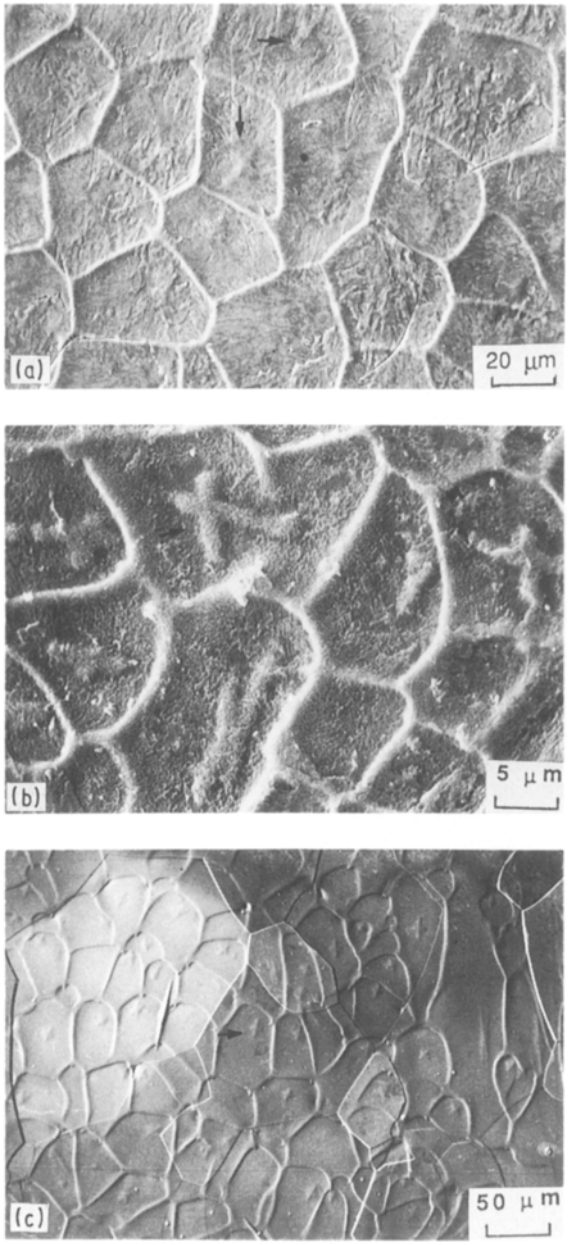

Figure 3 Secondary electron images of Fe–Ni alloys supercooled to 60 K at different Ni compositions, demonstrating the solute rich crosses inside the dendrite elements. (a) 15 wt % Ni; (b) 33.3 wt % Ni; and (c) 45 wt % Ni.

some particles can be seen in the interior of the γ plates. One such particle is marked by an arrow in Fig. 5. The electron-microscopic contrast of this particle can easily be changed with the tilt, indicating that the particle has crystalline structure. An enlarged area of a γ plate with a particle inside, and the corresponding selected diffraction pattern, are shown in Fig. 6. The selected area diffraction pattern (Fig. 6c) reveals two arrays of reflections, which are indexed in terms of a γ_{fcc} and an α_{bcc} unit cell with the lattice parameters $a_\alpha = 0.2875$ nm and $a_\gamma = 0.3591$ nm, respectively (see schematic diagram in Fig. 6d). Dark field photographs have shown that the bcc reflections arise from the particle marked by arrows in Fig. 6a. The dark field image of this particle taken with a $(0\,1\,1)_\alpha$ reflection is shown in Fig. 6b. X-ray microanalysis of this particle has shown that its composition is approximately the same as the composition of the liquid, while the rest of the γ plate has a lower Ni concentration of about 1 wt %.

A different solid state transformation was found in samples containing 33.3 wt % Ni as illustrated in Fig. 7. Fig. 7a to c show a series of transmission electron micrographs of Fe–33 wt % Ni alloys for different cooling paths starting at the liquid state: (a) the liquid sample was quenched into water from the liquid state (L); (b) the solid sample was quenched into water after slow cooling to 1100 °C in the levitation apparatus (solid state, S); and (c) the liquid sample was quenched into water after supercooling by ~ 130 K. The transmission electron photograph of a sample quenched into water from the liquid state is given in Fig. 7a. The thin plates which appear are matrix twins. The microstructure of the specimen quenched after the slow solidification in the levitation apparatus exhibits a twin structure, which is characteristic of fine coherent precipitates giving rise to the streaking effects seen in the diffraction pattern of Fig. 8. The coherent particles became much coarser for samples which were subjected to supercooling of 130 K prior to quenching, as evident in the bright field images of Fig. 7b and c, and from their corresponding selected area diffraction patterns. The diffraction pattern taken from the supercooled specimen exhibits similar streaking effects as shown in Fig. 8. The supercooled sample was further cooled to different temperatures in a cold stage. Only after reaching the liquid nitrogen temperature (77 K) could one observe a few martensite plates, with the majority of the sample remaining untransformed.

4. Discussion

As mentioned earlier [9, 10], the sub-grain morphology of supercooled Fe–Ni alloys may be classified into four categories. Each of the sub-grain morphologies contain fine microstructural details which depend on the solidification path and the composition. Supercooling has a great influence on the solidification path and hence on the nature of the solid state transformation. Our experimental results indicate that supercooling might influence the solid state transformation in two aspects: 1. It might cause alternative nucleation, giving rise to a different path of solid state transformation in the course of cooling down to room temperature; 2. It might cause coarsening of the coherent precipitation in Fe–33 wt % Ni compared with the conventional solidification.

4.1. Alternative nucleation and its influence on the martensitic transformation path

The results of the present study show that the microstructure also depends on the relative position of the nucleation temperature (T_n) with respect to the δ–T_o and γ–T_o temperatures (T_o denotes the mid-rib temperature, where the free energy of the solid is equal to the free energy of the liquid) – see Fig. 9. This is due to the fact that the two phases γ and δ can nucleate in these alloys depending on the supercooling [11], as can be seen from the iron-rich portion of the Fe–Ni

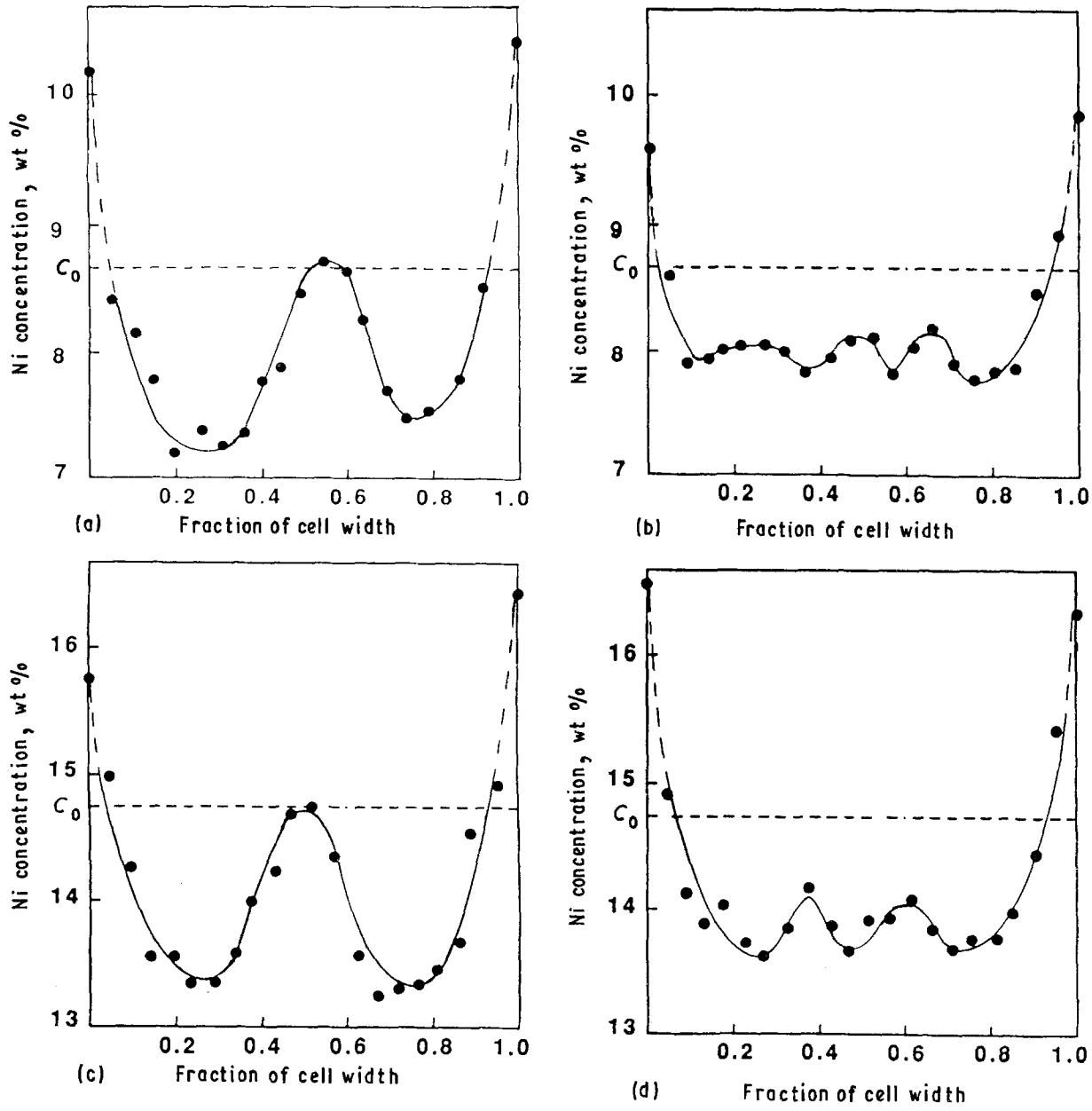

Figure 4 Ni concentration line profiles across dendrite elements for Fe–8.7 wt % Ni and Fe–14.7 wt % Ni alloys supercooled above (a, c) and below (b, d) the metastable extension of δ–T_0.

phase diagram in Fig. 9. In Fe–Ni alloys containing above 7 wt % Ni, the first solid to form during conventional solidification without undercooling is the γ–Fe phase. After solidification is completed upon cooling below the martensite-start temperature, M_s (which is a function of composition [1]), the γ–Fe phase undergoes a martensitic transformation (γ–Fe $\rightarrow$ α'–Fe). In the martensitic transformation, the γ–Fe phase (fcc) transforms to a mixture of approximately parallel α' (bcc) lath and γ–Fe (fcc) lath, which alternate sequentially. The α'–Fe and the γ–Fe phases have the same composition. When the M_s temperature is below room temperature (for over 28 wt % Ni), the γ–Fe phase becomes stable at room temperature. In alloys containing less than 6 wt % Ni, the first solid to form during conventional solidification (without supercooling) is the δ–Fe phase [11]. Upon further cooling the δ–Fe phase transforms to a γ–Fe, followed by a martensitic transformation according to the following equation: δ–Fe $\rightarrow$ γ–Fe $\rightarrow$ α'–Fe. The morphology of the martensite lath does not change when the Fe–Ni alloys are subjected to supercooling prior to nucleation. However, supercooling of Fe–Ni alloys might change the transformation sequence from δ–Fe to α–Fe.

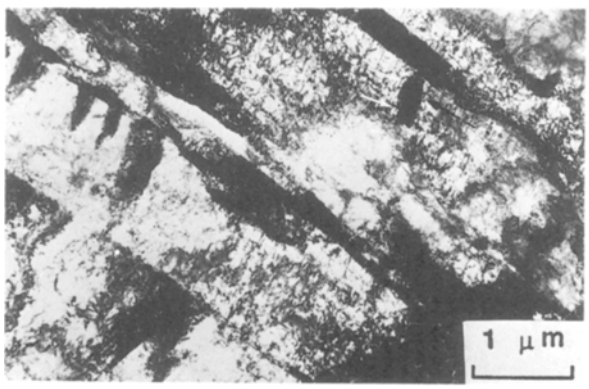

Figure 5 Transmission electron micrograph showing the microstructure of Fe–8 wt % Ni which was supercooled 210 K prior to quenching. An arrow marks some crystalline particles embedded in a γ–Fe lath.

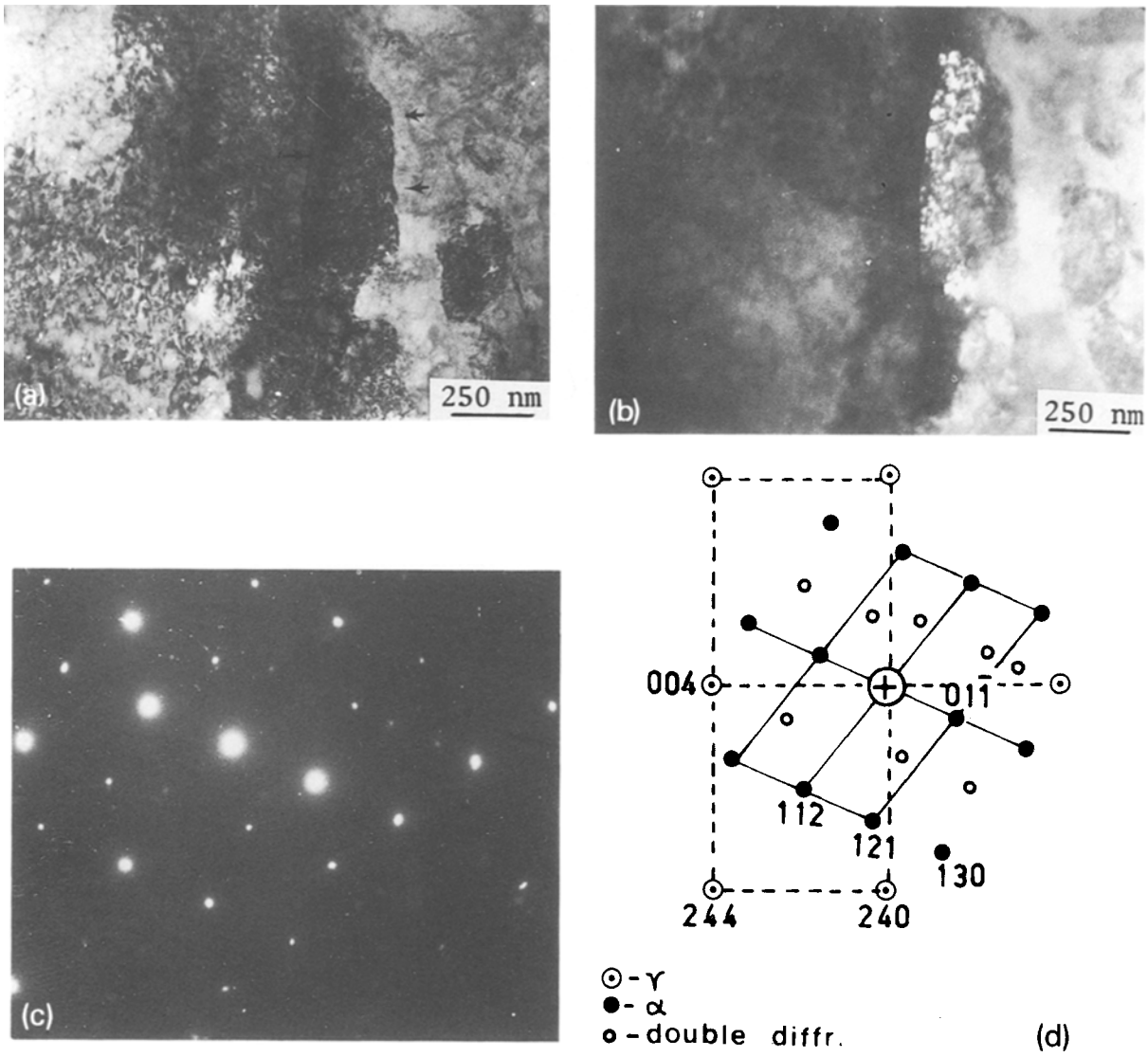

Figure 6 Transmission electron micrographs showing the bcc particle embedded in a γ–Fe lath. (a) Bright field image of the bcc particle; (b) dark field of the particle, taken with $(0\,1\,1)_\alpha$; (c) selected area diffraction pattern taken from the particle in Fig. 4a; and (d) Key diagram for the diffraction pattern in Fig. 4c. (⊙) γ; (●) α; (○) double diffraction.

In the case of the solidification of Fe–Ni alloys supercooled to a temperature between the liquidus temperature and γ–T_o, the first solid to form can only be the γ–Fe phase and solidification proceeds by a partition mode (i.e. the solid composition follows the solidus line and the liquid concentration follows the liquidus line). In alloys supercooled to a temperature between the γ–Fe solidus and the metastable extension of δ–T_o, the first solid to form is again the γ–Fe phase. However, in this case, solidification starts at a C_o composition (initial composition), as seen in the enlarged zone of Fig. 9b, and proceeds partitionlessly until recalescence increases the temperature to the level where partition occurs. The temperature at which partition starts is above the solidus temperature and may be as high as γ–T_o [11]. As recalescence proceeds, the temperature rises above γ–T_o and induces a solute partitioning.

When a Fe–Ni alloy is supercooled to a temperature, T_n, that is below δ–T_o, it is thermodynamically possible for the first nucleating solid to be a δ–Fe instead of a γ–Fe [11]. Such alternative nucleation of the δ–Fe phase is possible if the activation energy for the δ-phase nucleation is lower than for the γ-phase at the same supercooling level. We interpret the presence of a particle with a bcc structure embedded in a γ–Fe martensite lath (Figs 5 and 6) as experimental evidence that the alternative nucleation of a δ–Fe phase indeed occurs. Assuming that this particle originated from a γ–Fe phase, then the $\gamma \rightarrow \alpha'$ martensitic transformation would occur during cooling to ambient temperature and the particle would have a martensitic morphology with the Ni content equal to that of a γ–Fe phase. In fact, the particle does not possess a martensitic morphology, and has a somewhat rounded form. Further, the Ni-content in the particle is by about 1% larger than the Ni concentration in the surrounding γ-phase. The presence of such a bcc particle in the γ-lath can be readily explained by the alternative nucleation of the δ-phase. The particle with the bcc structure is the first to emerge from the liquid as a δ-bcc structure as a result of an alternative nucleation, and then the γ-phase forms around it. In the course of cooling, the γ-phase converts into a mixture of γ and α′ (martensite lath). The δ-particle, while remaining inside the γ-fcc region, has to transform into an α-bcc in one of two ways: (a) it transforms through a martensitic transformation ($\delta \rightarrow$

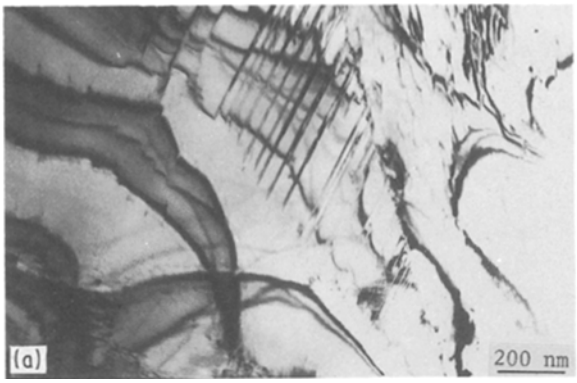

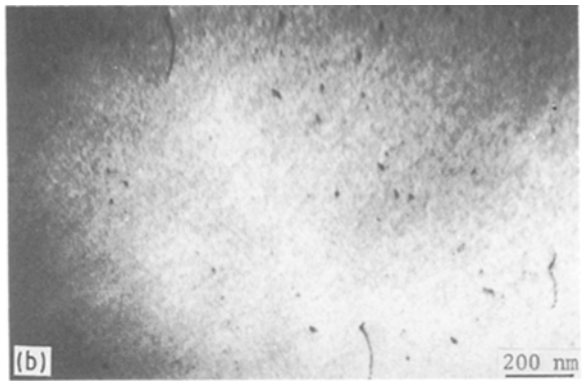

Figure 7 Transmission electron micrographs showing the microstructure of Fe–33 wt % Ni for different solidification paths. (a) Sample was quenched from the liquid state; (b) sample was quenched from the solid state; and (c) sample was supercooled to 130 K prior to quenching.

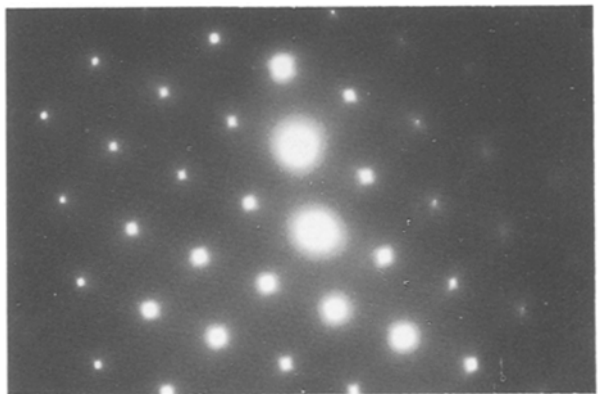

Figure 8 Selected area diffraction pattern taken from the twin structure shown in Fig. 7b. The faint streaks passing through the matrix reflection can be discerned.

$\gamma \rightarrow \alpha'$); or (b) it transforms directly from δ to α without going through in the γ state ($\delta \rightarrow \gamma$). Since the particle embedded in the γ-lath lacks a martensitic morphology, it might be that the second type of reaction is actually taking place.

The above results are in agreement with those by Cech [12] if we assume that the bcc-metastable phase obtained by Cech in the small size powder is a δ-phase resulting from an alternative nucleation.

It should be emphasized that in order to obtain the alternative crystallization, the sample has to be supercooled below δ–T_o. This temperature is a function of the alloy composition. According to the calculations made by Kelly and Vander Sande [11], the supercooling required for alternative crystallization in Fe–Ni alloys containing 7, 10, 15, 20, and 25 wt % Ni

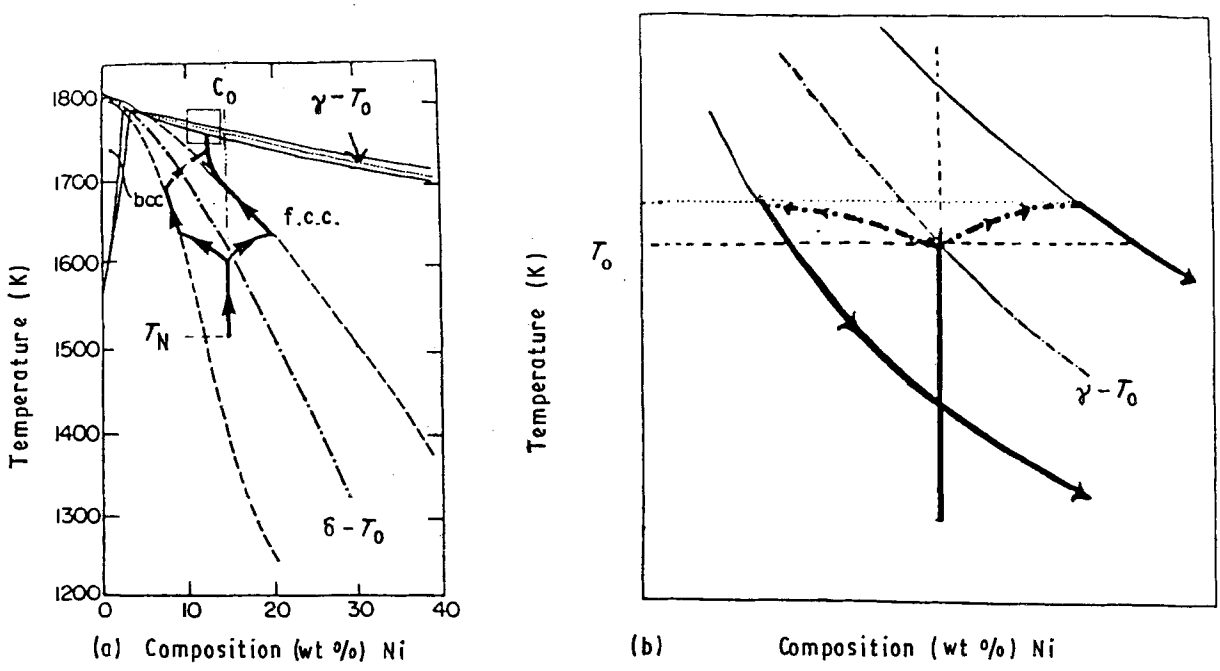

Figure 9 Partial Fe–Ni phase diagram illustrating the solidification paths of (a) nucleation below the metastable extension of δ–T_o; and (b) nucleation below γ–T_o but above the metastable extension of δ–T_o

are 40, 65, 155, 240, and 340 K, respectively. This may be the reason why, in previous studies where the supercoolings were less than 340 K, the alternative nucleation of the δ–Fe phase in Fe–25 wt % Ni samples has not been observed. Such a high degree of supercooling may be obtained only in a fine powder as in the case of Cech's experiments. Therefore, the observation of the δ–Fe phase in Cech's work is understandable.

4.2. Supercooling impact on solidification path.

Supercooling also has an influence on the solidification path as illustrated in Fig. 9. When the nucleation temperature, T_n, is lower than the metastable extension of δ–T_o (see Fig. 9a), the solidification path is rather complicated. First to solidify is the δ–Fe phase, as alternative nucleation becomes possible. This primary phase solidifies partitionlessly at the beginning but, as solidification proceeds, the temperature rises above the metastable extension of δ–T_o and partitioning begins. Above this temperature but below the metastable δ–liquidus extension, the δ–Fe phase will continue to grow but partitioning will occur. When the recalescence temperature rises above the metastable δ–solidus extension, the existing δ–Fe phase becomes unstable and tends to dissolve in the liquid or to transform into γ–Fe by a solid state massive transformation. Simultaneously, it might be possible for γ–Fe to nucleate on the existing δ–Fe via a peritectic reaction or directly through the liquid → solid transformation without any influence of the existing δ–Fe. The TEM observations (Figs 5 and 6) indicate that some residual δ–Fe phase did not have sufficient time to dissolve while the γ–Fe covers it and grows directly from the liquid. As long as the liquid temperature stays below γ–T_o, the γ phase grows partitionlessly. However, in such a situation, the liquid composition is changed due to dissolution of the Ni-poor δ–Fe phase. As soon as the temperature rises above γ–T_o, the γ–Fe continues to grow with partitioning. Since the growth and dissolution processes may occur together, one expects to have localized fluctuation in the solute profiles as indeed takes place (Fig. 4).

4.3. Solid state precipitation

Fe–33 wt % Ni, which solidified from a supercooled liquid, as well as alloys solidified in the levitation apparatus and dropped into water when already in the "solid" state, underwent coherent precipitation. Due to their very small dimensions it was impractical to perform X-ray elemental microanalysis. Kachi *et al.* [13] observed an anomalous peak at 800 °C in specific heat curves of Fe–Ni alloys containing 28 and 31 wt % Ni. After thermomagnetic and differential thermal analysis of those alloys they concluded that this anomaly could be accounted for by a superstructure of a Fe_3Ni composition. It might be that the coherent precipitation we have found in the present study is of Fe_3Ni particles. Our results suggests that the dimensions of the coherent particle depend on the solidification path, especially on supercooling. However, the explanation of this phenomenon is still inconclusive, and more experiments are desirable.

5. Summary

Scanning and transmission electron microscopy were used to investigate the impact of supercooling on microstructure, composition and solid state transformation in the Fe–Ni system. It was found that, irrespective of the supercooling degree, Fe–Ni samples containing a local composition between 7 and 28 wt % Ni underwent a martensitic transformation above room temperature. The martensite morphology is superimposed on the sub-grain microstructure obtained by supercooling. Solid state coherent precipitation was observed in Fe–33 wt % Ni alloys. It is likely that those precipitates are of a Fe_3Ni phase. The precipitation dimensions depend on the solidification path. The existence of those precipitates might explain the decrease of martensitic start temperature M_s to almost 77 K of Fe–33 wt % Ni alloys.

When nucleation temperature is below the metastable extension of δ–T_o, the alternative δ–Fe phase may nucleate and grow partitionlessly until the temperature increases above δ–T_o due to recalescence. The δ–Fe becomes unstable if the temperature exceeds the metastable extension of δ–liquidus. At this stage, δ may transform directly to γ, or γ–Fe may nucleate and absorb the dissolving δ–Fe particles. Since the growth and dissolution processes may occur together, one expects to have localized fluctuations in solute profiles. It should be noted that because the recalescence is very rapid, some particles of δ–Fe may remain undissolved and engulfed in the γ–Fe phase.

References

1. L. KAUFMAN and M. COHEN, *Trans. AIME, J. Metals* **October** (1956) 1393.
2. J. W. CHRISTIAN, in "The mechanism of phase transformation in crystalline solids", 3 to 5 July 1968, University of Manchester "Monograph and reports Series" No. 33. (Institute of Metals, London, 1968) p. 129.
3. R. I. PATTERSON and C. M. WAYMAN, *Acta Met.* **14** (1966) 347.
4. A. MUNITZ and G. J. ABBASCHIAN, in "Undercooled alloy phases ", edited by C. C. Koch and E. W. Collings (The Metallurgical Society of AIME, New Orleans, 1986) p. 23.
5. D. D. McDEVITT and G. J. ABBASCHIAN, in "Chemistry and physics of rapidly solidified materials", edited by B. J. Berkowitz and R. O. Scattergood (The Metallurgical Society of AIME, St. Louis, 1982) p. 49.
6. D. D. McDEVITT and G. J. ABBASCHIAN, *Microstruct. Sci.* **11** (1983) 125.
7. T. Z. KATTAMIS and M. C. FLEMINGS, *Trans. TMS-AIME* **236** (1966) 1523.
8. T. Z. KATTAMIS, *Z. Metallkunde* (1970) 856.
9. A. MUNITZ and G. J. ABBASCHIAN, *Adv. Mater. Mfg Processes*, **3** (1988) 419.
10. G. J. ABBASCHIAN and M. C. FLEMINGS,*Met. Trans. A* **14A** (1983) 1147.
11. T. F. KELLY and J. B. VANDER SANDE, in "Chemistry and physics of rapidly solidified materials", edited by B. J. Berkowitz and R. O. Scattergood (The Metallurgical Society of AIME, St. Louis, 1982) p. 28.
12. R. E. CECH, *Trans. AIME J. Metals* (1965) 585.
13. S. KACHI, Y. BANDO and S. HIGUCHI, Jpn *J. Appl. Phys.* **1** (1962) 307 .

Received 20 February
and accepted 3 December 1990